IL-27 neutralization enhances macrophage polarization and improves immune checkpoint efficacy

Quentin Glaziou[1], Laetitia Basset[2], Sènan d'Almeida[3], Pascale Pignon[4], Nabila Jabrane-Ferrat[1], Christophe Blanquart[5], Yves Delneste[6], Julie Tabiasco[1]

[1] Toulouse Institute for Infectious and Inflammatory Diseases (INFINITy), INSERM, CNRS, Toulouse III Paul Sabatier University, Toulouse, France

[2] Department of Pathology, University Hospital of Angers, Angers, Université d'Angers, Inserm UMR 1307, CNRS UMR 6075, Nantes Université, CRCI2NA, 49000, Angers, France.

[3] Viollier AG, Allschwil 4123, Switzerland

[4] Univ Angers, Nantes Université, INSERM, CNRS, CRCI2NA, SFR ICAT, Angers, France

[5] Nantes Université, Inserm UMR 1307, CNRS UMR 6075, Université d'Angers, CRCI2NA, F-44000 Nantes, France.

[6] Univ Angers, Nantes Université, INSERM, CNRS, CRCI2NA, SFR ICAT, Angers, France; University Hospital of Angers, Angers, France

Keywords

Tumor Microenvironment, Immunotherapy, Macrophages, Immune Checkpoint, IL-27

List of Abbreviations

A2AR : Adenosine A2A Receptor
Ab : Antibody
AMP : Adenosine Monophosphate
ANOVA : Analysis of Variance
ATP : Adenosine Triphosphate
BRET : Bioluminescence Resonance Energy Transfer
CCL : Chemokine Ligand
CCR : C-C Chemokine Receptor
CD : Cluster of Differentiation
CFDA-SE : Carboxyfluorescein Diacetate Succinimidyl Ester
COX : Cyclooxygenase
CTLA-4 : Cytotoxic T-Lymphocyte Antigen-4
DC : Dendritic Cells
DNase : Deoxyribonuclease
ECAR : Extracellular Acidification Rate
ECL : Enhanced chemiluminescence

ELISA : Enzyme Linked Immunosorbent Assay
EP2/4 : Prostaglandin E2 receptor 2/4
GAPDH : Glyceraldehyde 3-Phosphate Dehydrogenase
GM-CSF : Granulocyte Macrophage-Colony Stimulating Factor
gMFI : Geometric Mean of Fluorescence Intensity
ICI : Immune Checkpoint Inhibitors
IFNγ : Interferon Gamma
IL : Interleukine
LAG3 : Lymphocyte-Activation Gene 3
LPS : Lipopolysaccharide
mAbs : Monoclonal Antibodies
M-CSF : Macrophage-Colony Stimulating Factor
M-CM : Macrophages-Conditioned Medium
MDSC: Myeloid-Derived Suppressor Cells
MFI : Median Fluorescence Intensity
mRNA : Messenger RNA
MUC1 : Mucin-1
NK : Natural Killer
OCR : Oxygen Consumption Rate
OxPhos : Oxidative Phosphorylation
PBS : Phosphate-Buffered Saline
PCR : Polymerase Chain Reaction
PD-1 : Programmed Death 1
PDGF : Platelet-Derived Growth Factor
PD-L1 : Programmed cell Death-Ligand 1
PGE2 : Prostaglandin E2
PHA : Phytohemagglutinin
PTGS2 : Prostaglandin-endoperoxide Synthase 2
RFI : Relative Fluorescence Intensities
RNA : Ribonucleic Acid
RPMI : Roswell Park Memorial Institute
SEM : Standard Error of the Mean
TAM : Tumor-Associated Macrophages
TGFβ : Tumor Growth Factor β
Th1 : T helper 1
TIGIT : T cell Immunoreceptor with Ig and ITIM domains
TIM3 : T-cell Immunoglobulin and Mucin-domain containing 3

TME : Tumor Microenvironment

TNFα : Tumor necrosis factor alpha

Treg : T regulator cell

VEGF : Vascular Endothelial Growth Factor

Abstract

Tumor-associated macrophages (TAMs) accumulate in most solid tumors, where they secrete inflammatory cytokines and growth factors that promote tumor progression, immune evasion, and angiogenesis. TAMs have recently emerged as therapeutic targets for reactivating antitumor immunity and restraining tumor progression. In this study, we investigated whether IL-27 neutralization could modulate macrophage polarization and thereby alter the tumor immune microenvironment.

The effects of IL-27 neutralization were examined using complementary in vitro and in vivo approaches. In vitro, human macrophages were analyzed by flow cytometry, qRT-PCR, ELISA, and Western blot to assess changes in their immunoregulatory profile. In vivo, the MC38 murine colon adenocarcinoma model was used to evaluate the impact of IL-27 blockade on the tumor immune microenvironment.

Our findings highlight a key role for IL-27 in promoting the immunosuppressive phenotype of human macrophages. Mechanistically, IL-27 neutralization diminished macrophage-mediated suppression by reducing cytokine production and the expression of immunoinhibitory surface molecules. These modifications led to a reduction in the ability of macrophages to inhibit the function of CD4□ and CD8□ T cells. Furthermore, in vivo neutralization of IL-27 attenuated MC38 tumor growth and enhanced the efficacy of immune checkpoint therapy.

Collectively, targeting IL-27 promoted macrophage repolarization and enhanced CD4□ and CD8□ T cell responses. These findings suggest that IL-27 neutralization is a promising therapeutic strategy to reprogram macrophages in the tumor microenvironment (TME) and improve the clinical efficacy of cancer immunotherapy.

Introduction

The clinical development of immune checkpoint inhibitors (ICIs) has dramatically transformed cancer treatment. However, despite the remarkable success of ICIs, many patients fail to achieve durable responses as tumors develop mechanisms of resistance (1). One major cause of resistance is the accumulation of immunosuppressive factors in the tumor microenvironment (TME) (2). Indeed, established tumors are often dominated by immunosuppressive cells, including regulatory T cells, regulatory macrophages, and myeloid-derived suppressor cells (MDSCs), along with various immunosuppressive mediators (e.g., IL-10, TGFβ, CCL22, CCL17, CCL2, prostaglandin E2, adenosine, M-CSF) (3,4). Modulating the TME is therefore an appealing therapeutic strategy, but the multitude of pro-tumoral factors present makes broad targeting challenging (4). One feasible approach is to re-educate specific immune cells within the TME toward an anti-tumor phenotype.

Macrophages, often referred to as tumor-associated macrophages (TAMs) in the context of cancer, are among the most abundant immune cells in solid tumors and generally correlate with poor prognosis (5,6). In established tumors, TAMs typically acquire an immunoregulatory (M2-like) phenotype that supports tumor growth (6,7) . These immunosuppressive macrophages secrete pro-angiogenic factors

(e.g., VEGF, PDGF) and recruit other cells (e.g., monocytes, regulatory T cells) by releasing chemokines (CCL2, CCL17, CCL22) and immunosuppressive cytokines (IL-10, TGFβ), while also expressing cell-surface molecules such as CD39, CD73, PD-L1, and CD155 that further dampen anti-tumor immunity (8). Owing to this multifaceted influence on tumor progression, TAMs are at the center of new therapeutic strategies aiming to improve anti-cancer immune responses (9).

Recent studies in various tumor models suggest that inhibiting TAM accumulation or activation can slow tumor progression (9–11). However, rather than simply depleting macrophages, reprogramming immunosuppressive TAMs toward a pro-inflammatory, anti-tumor state (often termed “re-education”) may be more effective in unleashing anti-tumor immunity (9,11–15). TAMs (like all macrophages) exhibit a high degree of functional plasticity, capable of both pro-inflammatory and anti-inflammatory function depending on signals from the surrounding tissue microenvironment . Indeed, we and other previously demonstrated that targeting the ectonucleotidase CD39 on macrophages enhanced their inflammatory phenotype and function (16,17). CD39 is an ectonucleotidase that hydrolyzes extracellular pro-inflammatory ATP into AMP, which is subsequently converted by CD73 into adenosine, a potent immunosuppressive metabolite (18–23). Thus, CD39, CD73 and adenosine contributes to the establishment of an immunosuppressive tumor microenvironment and has therefore emerged as a promising therapeutic target in oncology (21–24,24,25). We and others showed that the expression of CD39 and the production of the anti-inflammatory cytokine IL-10 by immune cells (including macrophages) are highly dependent on interleukin-27 (IL-27) signaling (16,20,26,27). IL-27 is a pleiotropic cytokine with complex roles in immunity: it can promote antitumor immune responses in some contexts while driving immune escape in others (28–32). For example, IL-27 has been reported to enhance cytotoxic T lymphocyte activity and upregulate co-inhibitory molecules on T cells and tumor cells (33,34). By contrast, its influence on TAM polarization remains poorly characterized, even though TAMs are key regulators of the TME.

Based on this background, we hypothesized that neutralizing IL-27 could skew macrophages from an immunosuppressive toward an immunostimulatory phenotype, thereby improving anti-tumor immunity. In the present study, we evaluated the impact of IL-27 neutralization on human macrophage polarization in vitro, as well as on the tumor immune microenvironment in vivo using a murine colon carcinoma model. Our results demonstrate that blocking IL-27 drives human macrophages toward a less suppressive, more pro-inflammatory state, characterized by reduced expression of immunosuppressive molecules and enhanced T cell-stimulatory capacity. Furthermore, IL-27 blockade in vivo led to slower tumor growth and improved efficacy of PD-L1 checkpoint inhibition. These findings provide new insight into the role of IL-27 in macrophage plasticity and highlight IL-27 as a promising immunotherapeutic target for cancer.

Materials and Methods

Cell Culture

CD14□ monocytes and CD4□/CD8□ T cells were isolated from healthy donor peripheral blood mononuclear cells by positive selection (Miltenyi Biotec). Monocytes were differentiated into macrophages by culturing them for 7 days in RPMI 1640 with 10% fetal bovine serum and 50 ng/mL macrophage colony-stimulating factor (M-CSF) (ORF Genetics, Iceland), a standard concentration for human macrophage generation (35,36). In parallel, a subset of monocytes was differentiated with 50 ng/mL granulocyte–macrophage colony-stimulating factor (GM-CSF) to generate pro-inflammatory macrophages for comparison. IL-27-neutralizing antibody (5 µg/mL; R&D Systems, AF-2526, goat IgG) or isotype control antibody (5 µg/mL; R&D Systems, AB-108-C, goat IgG) was added to monocyte cultures on the day of plating and on day 3 to generate IL-27-neutralized macrophages (Mα27) and isotype control-treated macrophages (Miso), respectively. Where indicated, caffeine (Sigma-Aldrich; 10 µM) or the EP2 receptor antagonist AH6809 (Cayman Chemical; 10 µM) was added during differentiation at the specified concentrations.

Cell Activation Assays

For macrophage activation, differentiated macrophages were plated at 2×10^5 cells per well in flat-bottom 96-well plates and stimulated with lipopolysaccharide (LPS, E. coli O111:B4; 200 ng/mL; Sigma-Aldrich). Immediately before LPS stimulation, macrophages were extensively washed (3× with pre-warmed PBS [Ca^{2}□/Mg^{2}□-free] and once with complete medium) to remove any residual neutralizing or isotype antibodies from the differentiation phase. Purified CD4□ and CD8□ T lymphocytes were seeded in 96-well plates at a density of 2 × 10□ cells per well and stimulated with phytohemagglutinin (PHA, 10 µg/mL; Sigma-Aldrich) in antibody-free medium. Stimulation was performed either in the absence or presence of 10% macrophage-conditioned medium (M-CM). M-CM corresponded to supernatants collected after 24 h of LPS activation of Mα27 or Miso macrophages, prepared under antibody-free conditions as described above. Culture supernatants were collected after 48 h and stored at –80 °C prior to cytokine analysis by ELISA.

For T cell proliferation assays, CD4□ T cells were labeled with 3 µM CFDA-SE (Invitrogen) and cultured (2×10^5 cells per well) in 96-well plates pre-coated with anti-CD3 antibody (1 µg/mL, clone OKT3; ATCC). Soluble anti-CD28 (1 µg/mL; BD Pharmingen) was added to provide co-stimulation. Macrophage influence was tested by adding 50% (v/v) of M-CM from 24 h LPS-activated Mα27, Miso, or macrophage without antibody addition (untreated macrophages) cultures (all M-CM generated after the extensive washing step and in antibody-free medium). After 6 days, CD4□ T cell proliferation was assessed by flow cytometry based on CFDA-SE dilution.

For CD8□ T cell cytotoxicity assays, a luciferase-expressing MUC1□ murine mesothelioma cell line (Meso34) was co-cultured with a MUC1-specific CD8□ T cell clone (37) (1×10^5 T cells with 3×10^4 target cells) in the presence or absence of macrophages (2×10^4 Mα27 or Miso). Before co-culture, macrophages were thoroughly washed as above and resuspended in antibody-free assay medium to preclude any antibody carryover. Co-cultures were maintained for 72 h. Tumor cell killing

was quantified by measuring luciferase activity released into the supernatant, which correlates with tumor cell lysis.

Across all functional assays, “Miso” macrophages served as isotype-exposed controls during differentiation, and no anti–IL-27 or isotype IgG was present during LPS activation, in the conditioned media, or during T cell co-culture. These procedures ensure that differences between Mα27 and Miso reflect macrophage-derived factors and phenotype rather than direct antibody effects.

Soluble Mediator Analysis

Concentrations of cytokines and other mediators in culture supernatants were measured by ELISA according to the manufacturers’ protocols. The following kits were used: human IL-10, IL-2, IFN-γ (Diaclone); human CCL2, CCL22, prostaglandin E□ (PGE□), IL-27 (R&D Systems). For the quantification of membrane-associated IL-27, cell pellets were subjected to five freeze–thaw cycles, resuspended in PBS, disrupted by sonication, and centrifuged at $10^5 \times g$ for 10 min. The clarified supernatants were subsequently used for ELISA analysis.

Western Blotting

Macrophage cell lysates (1×10^6 cells per sample) were prepared in RIPA lysis buffer with protease/phosphatase inhibitors. Equal amounts of protein were separated by SDS-PAGE and transferred to PVDF membranes. Blots were probed with primary antibodies against human COX-2 and CD73 (both 1 µg/mL; Cell Signaling Technology), followed by HRP-conjugated secondary antibodies (anti-rabbit IgG or anti-mouse IgG, 1 µg/mL; Cell Signaling). β-actin (1 µg/mL; Cell Signaling) was used as a loading control. Bands were visualized using ECL or SuperSignal West Femto chemiluminescent substrate (Thermo Fisher).

Gene Expression Analysis

Total RNA was extracted using the RNeasy Mini kit (Qiagen) and reverse-transcribed with Superscript II (Thermo Fisher). Quantitative PCR was performed using SYBR Green Supermix (Bio-Rad) on a CFX96 thermocycler (Bio-Rad). Primer sequences (e.g., for IL10, NT5E/CD73, PTGS2/COX-2) are available on request. Gene expression was calculated by the $2^{(-\Delta Ct)}$ method, normalizing to GAPDH as a housekeeping gene.

Metabolic Assays

Macrophage metabolic function was assessed using a Seahorse XFe24 Analyzer (Agilent). Oxygen consumption rate (OCR) was measured with the Seahorse Mito Stress Test, and extracellular acidification rate (ECAR) was measured with the Glycolysis Stress Test, following the manufacturer’s protocols. Macrophages were plated at 1×10^5 cells per well in Seahorse plates and sequentially treated with oligomycin, FCCP, and rotenone/antimycin A (for OCR assays) or glucose, oligomycin, and 2-deoxyglucose (for ECAR assays). Parameters of mitochondrial respiration (basal OCR, maximal OCR, ATP-linked OCR) and glycolysis (basal ECAR, glycolytic capacity) were derived. Lactate production was measured in 24 h culture supernatants (from 1×10^5 cells per well) using a colorimetric L-lactate assay kit (Abcam).

In Vivo Tumor Model

The MC38 murine colon adenocarcinoma cell line was maintained in culture and harvested during log-phase for injection. Female C57BL/6 mice (8 weeks old) were injected subcutaneously in the right flank with 5×10^5 MC38 cells in 100 µL PBS. Once tumors became detectable in all mice (approximately 8–10 days post-injection), animals were randomly divided into two groups. One group received an IL-27-neutralizing antibody (anti-mouse IL-27p28, clone MM27-7B1, Ultra-LEAF purified; BioLegend), while the other received a non-relevant isotype control antibody of the same IgG subclass (Mouse IgG2a, κ Isotype Control, Clone: MOPC-173, Ultra LEAF purified; Biolegend). Treatments were administered intratumorally every 48 hours for a total of five doses, each consisting of 20 µg in 20 µL per injection. Starting two days after the final anti-IL-27 injection, an anti-PD-L1 antibody (clone 10F.9G2, InVivoMab; BioXcell) was given intraperitoneally (200 µg in 200 µL per injection) every three days for three doses. Tumor growth was monitored every two days using calipers. Tumor volume was calculated as (length × width × height) × 0.52 ("0.52" comes from π/6 for an ellipsoid approximation). Tumor measurements were performed by two independent researchers, one of whom was blinded to the treatment groups. Mice were euthanized when tumor volume exceeded 1,800 mm^3 or if tumors ulcerated.

Flow Cytometry

Human macrophages

Macrophages were stained with fluorochrome-conjugated antibodies (Supplementary Table 1). Non-viable events were excluded with 7-AAD (BioLegend, San Diego, CA, USA). Acquisition was performed on a BD FACSCanto flow cytometer (BD Biosciences, San Jose, CA, USA). Data were analyzed in FlowJo v10.9 (FlowJo LLC). Median fluorescence intensity (MFI) values for each marker were normalized to the MFI of the corresponding isotype control on the same sample, yielding a relative fluorescence intensity (RFI). These RFI values were used to compare expression between Mα27 and Miso conditions.

Tumor-infiltrating cells

Tumors were minced with scissors and enzymatically dissociated (collagenase IV + DNase I, 20 min, 37 °C). Cells were washed and passed through 200 µm strainers, then stained with LIVE/DEAD Fixable Yellow (Thermo Fisher Scientific) to exclude non-viable events. Fc receptors were blocked (FcR Block, Miltenyi Biotec, Germany) before surface staining with the antibody panels listed in Supplementary Table 1. Multiparameter flow cytometry was performed on a BD LSRFortessa (BD Biosciences). Median fluorescence intensities (MFIs) were calculated on viable cells; data were analyzed in FlowJo v10 (FlowJo LLC).

Statistics

Statistical analyses were performed in GraphPad Prism 10 (GraphPad Software, San Diego, CA, USA). Two-group comparisons used the Mann–Whitney U test. For comparisons involving three or more groups, one-way ANOVA with Tukey's multiple-comparisons test was applied. Survival curves

were compared using the log-rank (Mantel–Cox) test. All tests were two-sided, and statistical significance was set at $\alpha = 0.05$ ($p < 0.05$; *$p < 0.01$; **$p < 0.001$). In the graphical representations, only statistically significant differences directly relevant to the discussion were displayed. Results not reaching statistical significance but showing a consistent pattern were reported in the text and described as trends.

Results

IL-27 neutralization during macrophage differentiation reduces immunosuppressive properties

Prior to performing neutralization experiments with a specific antibody, we confirmed IL-27 expression by monocyte (before any differentiation step and without exogenous stimulation) and its release into culture supernatants during differentiation. RT-qPCR analysis showed the presence of transcripts encoding both IL-27 subunits, IL-27p28 and Ebi3, which together form the biologically active heterodimer (Supplementary Figure 1A). Transcripts for both receptor subunits, IL-27RA and gp130, were also detected in monocytes (Supplementary Figure 1A). The expression of IL-27p28 and IL-27 RA is maintained after 5 days of culture in the presence of M-CSF (Supplementary Figure 1B).
We next examined IL-27p28 protein in culture supernatants in the absence or presence of LPS stimulation. IL-27 was undetectable in supernatants from unstimulated monocytes or after 5 days of differentiation (Figure S1C). By contrast, LPS stimulation induced a detectable IL-27p28 (Supplementary Figure 1C). Since IL-27RA and gp130 transcripts were present in these cells, we hypothesized that IL-27p28 secreted by unstimulated monocytes could bind to their cognate receptors at the cell surface. Indeed, quantification of membrane-associated IL-27p28 confirmed its presence under these conditions (Supplementary Figure 1D).
Finally, we monitored IL-27p28 secretion during macrophage differentiation from day 0 to day 5 in the presence of M-CSF. IL-27p28 concentration increased progressively over the course of differentiation (Supplementary Figure 1E).

To assess the impact of IL-27 on macrophage polarization, we differentiated human monocytes with M-CSF (50 ng/mL) and neutralized IL-27 throughout this process. Consistent with our previous findings (16), macrophages differentiated with IL-27 neutralization (Mα27) showed significantly reduced CD39 expression compared to isotype-treated controls (Miso). Flow cytometry confirmed that surface CD39 protein levels were lower on Mα27 cells than on Miso cells, and qRT-PCR analysis similarly revealed a decrease in ENTPD1 (CD39) transcripts in Mα27 (consistent with ref. 16; data not shown). Because adenosine signaling is linked to CD39 function in TAMs, we next tested whether disrupting adenosine signaling would similarly affect CD39 expression. Indeed, adding caffeine, a non-selective adenosine receptor antagonist, during macrophage differentiation significantly decreased surface CD39 levels (Supplementary Figure 2A), supporting the role of adenosine in maintaining $CD39^{high}$ immunosuppressive macrophages (17).

We next examined CD73, the cell-surface ectoenzyme that converts AMP (the product of CD39) into adenosine. IL-27 neutralization led to significantly lower CD73 surface expression on Mα27 macrophages compared to Miso controls (Figure 1A, 1B). This decrease was also evident at the transcript level: qRT-PCR showed that NT5E (CD73) mRNA was reduced in Mα27 cells relative to Miso (Supplementary Figure 3A). Together with our previous report (16), these results indicate that IL-27 signaling promotes high expression of both ectonucleotidases in the adenosine pathway (CD39 and CD73). Consequently, blocking IL-27 during macrophage differentiation downregulated both CD39 and CD73, potentially limiting the cells' capacity to generate immunosuppressive adenosine.

While we previously showed that IL-27 neutralization reduces PD-L1 expression on human macrophages(16), we now also find that IL-27-neutralized macrophages display diminished CD155 expression (Figure 1C). CD155 (PVR) is an immune checkpoint ligand that interacts with receptors such as TIGIT on T and NK cells, typically delivering an inhibitory signal (38–40). In cancers, high CD155 expression is associated with T cell dysfunction and resistance to immunotherapy (38,41). In our experiments, Mα27 macrophages showed roughly a 25% reduction in CD155 surface levels compared to Miso (Figure 1C).

Conversely, IL-27 neutralization increased the expression of several co-stimulatory or pro-inflammatory surface molecules on macrophages. Mα27 cells had significantly higher levels of CD80 and CD40 than Miso cells (Figure 1D, 1E). CD80 provides a co-stimulatory signal to T cells (via CD28) and is typically associated with classically activated M1 macrophages. CD40, a TNF receptor family member, is an activation-induced molecule on macrophages and dendritic cells that can license these cells to better prime T cells via CD40L interactions (42). We also observed a moderate but significant increase in CD48 on Mα27 macrophages (Figure 1F). CD48 can function as an activating receptor on immune cells and engage CD244 (2B4) on NK/T cells to promote immune activation in certain contexts (7).

In addition to cell surface markers, we analyzed the secretion of key immunoregulatory mediators by macrophages. Without LPS stimulation, Mα27 macrophages secreted significantly less CCL2 than Miso macrophages (Figure 1G). CCL2 is a chemokine that recruits monocytes to tumors, where they can differentiate into TAMs; thus, lower baseline CCL2 in Mα27 suggests a less chemoattractant, pro-tumoral profile. Upon LPS activation, however, Mα27 secreted more CCL2 than Miso (Supplementary Figure 3B), a pattern similar to inflammatory macrophages which produce little CCL2 at rest but upregulate it during activation (Supplementary Figure 3C). Another chemokine, CCL22, which recruits CCR4 regulatory T cells, was found at significantly lower levels in supernatants from Mα27 versus Miso macrophages (Figure 1H). Notably, IL-27 produced by dendritic cells has been shown to induce CCL22 and facilitate Tregs accumulation in tumors (43), suggesting that IL-27-neutralized macrophages might be less effective at attracting Tregs.

We confirmed that IL-27-neutralized macrophages produce less IL-10 upon LPS activation than controls (Supplementary Figure 3D), consistent with our previous report (16). IL-10 is a key

immunosuppressive cytokine associated with M2-like macrophages, so its reduction further indicates an attenuated regulatory phenotype in Mα27 cells. On the other hand, we examined two factors that can modulate anti-tumor immunity: prostaglandin E□ (PGE□) and GM-CSF.

PGE□, generally immunosuppressive in the TME, is involved in TAM development (44); inhibiting PGE□ signaling via EP2 receptor antagonist AH6809 significantly reduced CD39 levels during macrophage differentiation (Supplementary Figure 2B). We found that LPS-stimulated Mα27 macrophages secreted substantially less PGE□ than Miso (Figure 1I). Correspondingly, expression of cyclooxygenase-2 (COX-2, PTGS2), the enzyme responsible for PGE□ synthesis, was markedly downregulated in Mα27 at both the mRNA and protein levels (Supplementary Figures 3E, 3F, 3G). This suggests that IL-27 blockade skews macrophages away from a COX-2^{high}, PGE□-producing state.

GM-CSF is a cytokine that can drive monocytes toward dendritic cell differentiation and is linked to improved antigen presentation. We observed that Mα27 macrophages secreted significantly more GM-CSF than Miso upon LPS stimulation (Figure 1J). Notably, adding a low dose of GM-CSF during M-CSF-driven differentiation drastically reduced CD39 expression (Supplementary Figure 2C), consistent with GM-CSF's role in promoting a pro-inflammatory macrophage program (45). The elevated GM-CSF production by Mα27 cells may thus amplify local immune activation (by recruiting/activating dendritic cells, for example).

Collectively, these results demonstrate that IL-27 neutralization during human macrophage differentiation induces a broad phenotypic shift: reduced expression of immunosuppressive molecules (CD39, CD73, CD155, IL-10, CCL22, PGE□/COX-2) and increased expression of immunostimulatory molecules (CD80, CD40, CD48, GM-CSF, and inducible CCL2). A heatmap summarizing these changes is shown in Figure 1K. Overall, targeting IL-27 yielded macrophages with significantly diminished immunosuppressive properties.

IL-27 neutralization alters macrophage metabolism toward a pro-inflammatory profile

Cellular metabolism is closely tied to macrophage activation status. Inflammatory activation of murine macrophages typically suppresses oxidative phosphorylation (OxPhos) while enhancing glycolysis, driven by TCA-cycle rewiring (succinate/citrate, itaconate) and nitric oxide–mediated respiratory inhibition. In humans, this split is less stark, glycolysis often rises without loss of substantial OxPhos, highlighting bioenergetic plasticity (46). Metabolic programming is therefore a key determinant of immune function (47–49).

As a baseline comparison, we first characterized metabolic differences between GM-CSF–differentiated macrophages and M-CSF–differentiated macrophages. Consistent with a more activated phenotype, GM-CSF macrophages had significantly higher basal OCR (oxygen consumption in the resting state) and ATP-linked OCR than M-CSF macrophages (Figure 2A, 2B). This indicates that GM-CSF-conditioned macrophages were more metabolically active at rest, engaging oxidative phosphorylation to a greater degree. Interestingly, maximal OCR (mitochondrial respiratory capacity)

did not differ between GM-CSF and M-CSF groups (Figure 2C), suggesting GM-CSF macrophages utilize more of their mitochondrial capacity at baseline without necessarily having greater total capacity. We also found that GM-CSF macrophages displayed higher basal ECAR (glycolytic rate) and glycolytic capacity compared to M-CSF macrophages (Figure 2D, 2E). Correspondingly, GM-CSF macrophages produced more lactate in culture (Figure 2F). Thus, GM-CSF-derived macrophages had elevated utilization of both oxidative and glycolytic pathways relative to M-CSF macrophages, aligning with a more pro-inflammatory metabolic profile.

We then assessed the metabolism of IL-27-neutralized versus control antibody M-CSF macrophages. Even though both groups were generated with M-CSF, IL-27 neutralization significantly altered their metabolic state. Mα27 macrophages showed higher basal OCR than Miso, indicating enhanced mitochondrial respiration (Figure 2G). There was also a trend toward increased basal ECAR (glycolysis) in Mα27 (Figure 2H), though this did not reach significance. Importantly, ATP production (estimated from the oligomycin-sensitive OCR) was significantly greater in Mα27 compared to Miso (Figure 2I), as was lactate secretion (Figure 2J). The latter indicates a higher glycolytic flux in Mα27 cells. Together, these data suggest that IL-27-neutralized macrophages are more energetically active, with a metabolism shifted somewhat toward that of pro-inflammatory macrophages. Indeed, the metabolic differences between Mα27 and Miso (higher OCR, higher lactate) mirrored the direction of change seen between GM-CSF and M-CSF macrophages. These results imply that IL-27 blockade drives metabolic reprogramming consistent with macrophage activation and may support the functional changes (e.g., greater cytokine production) observed in Mα27 cells.

IL-27-neutralized macrophages better support T cell activation and cytotoxicity

The phenotypic and metabolic reprogramming of macrophages by IL-27 neutralization suggested that these cells might be less suppressive toward T cells. First, we examined CD8□ T cell effector function in the presence of M-CM. When activated CD8□ T cells were cultured with 10% of control M-CM , their secretion of IFN-γ was almost completely inhibited (Supplementary Figure 4A) indicating that factors produced by control macrophages can strongly suppress CD8□ T cells. By contrast, under the same conditions, CD8□ T cells cultured with supernatant from activated Mα27 macrophages secreted significantly more IFN-γ than those with Miso supernatant (Figure 3A). Although IFN-γ production was still reduced relative to T cells with no macrophage supernatant (Supplementary Figure 4A), the suppression was markedly less severe with Mα27-conditioned medium. This finding suggests that IL-27-neutralized macrophages produce fewer soluble suppressive factors that inhibit CD8□ T cell cytokine release. To preclude antibody-related artifacts, macrophages were extensively washed immediately before the 24-h LPS activation used to generate M-CM, thus, the differences observed in T-cell readouts reflect macrophage-derived factors rather than antibody carryover.

Next, we investigated the effect of macrophages on CD8□ T cell cytotoxicity using an in vitro tumor cell killing assay. In the absence of macrophages, the MUC1-specific CD8□ T cells efficiently lysed the MUC1□ tumor cells (50). Adding Miso macrophages to the co-culture reduced the overall cytotoxicity of the T cells (approximately a 10% decrease in tumor cell killing compared to no macrophage; Figure 3B). In contrast, adding Mα27 macrophages did not impair CD8□ T cell cytotoxicity; the lysis levels remained comparable to the no-macrophage condition (Figure 3B). Moreover, in direct comparison, activated Mα27 macrophages were significantly less suppressive than activated Miso macrophages, resulting in ~19% higher T-cell cytotoxicity in the presence of Mα27 (Figure 3B). These results indicate that IL-27-neutralized macrophages, unlike control macrophages, do not inhibit CD8□ T cell tumor-killing capacity. All assays were performed under the same washed/isotype-controlled conditions described above.

CD4□ helper T cells are critical for sustaining CD8□ T cell responses, partly through IL-2 production. We therefore examined IL-2 secretion by CD4□ T cells in the presence of M-CM. After 48 h of anti-CD3/CD28 stimulation, CD4□ T cells secreted nearly twice as much IL-2 when cultured with supernatant from activated Mα27 macrophages compared to supernatant from Miso macrophages (Figure 3C). This suggests that factors from IL-27-neutralized macrophages are less inhibitory (or possibly more supportive) to CD4□ T cell activation. In line with this, we assessed CD4□ T cell proliferation over 6 days by CFDA-SE dilution. We found that M-CM from activated Mα27 macrophages caused a significantly smaller reduction in the CD4□ T cell replication index than M-CM from activated Miso or from untreated macrophages (Figure 3D). In other words, CD4□ T cells proliferated more robustly in the presence of factors from IL-27-neutralized macrophages. As above, these experiments were conducted after thorough macrophage washing and with matched isotype controls in all conditions.

These experiments demonstrate that IL-27 neutralization endows macrophages with a diminished capacity to suppress T cell responses. CD8□ T cells maintain higher IFN-γ production and cytotoxic function, and CD4□ T cells exhibit greater IL-2 secretion and proliferation, in the context of Mα27 versus Miso macrophages. This improved support for T cell activity is consistent with the reduced output of immunosuppressive mediators (e.g., IL-10, PGE□) and increased output of supportive factors (e.g., GM-CSF) by IL-27-neutralized macrophages.

In vivo IL-27 neutralization delays tumor growth and prolongs survival

Encouraged by the in vitro results, we next assessed the effects of IL-27 neutralization in vivo using the MC38 colon tumor model. Mice bearing established MC38 tumors were treated with intratumoral anti-IL-27 antibody or control IgG (Figure 4A). IL-27 blockade resulted in significantly slower tumor growth compared to the control treatment (Figure 4B, 4C). By day 10, IL-27-neutralizing antibody treatment significantly delayed tumor growth relative to mice receiving an isotype control (Fig. 4B–C). Tumor growth curves diverged as early as 6 days after starting treatment, indicating a relatively rapid effect of IL-27 neutralization (Figure 4D). Furthermore, IL-27 antibody-treated mice showed a

survival benefit. The median survival in the anti-IL-27 group was 18.5 days, compared to 14 days in controls (Figure 4C). This extension of survival was statistically significant (log-rank $p = 0.008$). Thus, neutralizing IL-27 in the TME can impede tumor progression and modestly improve survival even as a single agent.

We then evaluated whether IL-27 neutralization could enhance the efficacy of PD-L1 checkpoint blockade, as our in vitro data suggested it might. A separate cohort of tumor-bearing mice was treated with anti-IL-27 as above, and then received anti-PD-L1 antibody beginning two days after the last IL-27 dose (Figure 5A). As shown in Figure 5B, the combination of IL-27 neutralization plus PD-L1 blockade led to greater tumor growth inhibition than either treatment alone. By the end of the observation period, tumors in the combination group were significantly smaller than tumors in mice that received control IgG of each treatment antibody, and they tended to be smaller than tumors in mice that received anti-PD-L1 alone (Figure 5B). Each monotherapy demonstrated efficacy compared with control treatments, while the combination of anti-IL-27 and anti-PD-L1 suggested an additional benefit, as survival curves indicated a tendency toward prolonged survival relative to anti-PD-L1 alone (Figure 5C). These findings suggest that IL-27 neutralization can set the stage for a more effective response to checkpoint inhibition.

In summary, IL-27 blockade in vivo slows tumor growth and can enhance the therapeutic effect of PD-L1 blockade. These outcomes are consistent with the idea that targeting IL-27 helps overcome immunosuppression in the TME, thereby improving anti-tumor immunity and response to ICIs.

IL-27 blockade modulates the tumor immune microenvironment

To understand how IL-27 neutralization was affecting immune cells in the tumor, we analyzed immune infiltrates from treated versus control tumors at day 10 of therapy. We focused on CD39 expression across various cell types, given CD39's role in generating immunosuppressive adenosine and its regulation by IL-27. Overall, IL-27-neutralized tumors exhibited lower levels of CD39 on infiltrating myeloid cells compared to controls (Figure 6A). In particular, mean CD39 expression (MFI) was reduced on tumor-infiltrating monocytes, dendritic cells (DCs), and neutrophils in the anti-IL-27 group (Figure 6A). This reduction was significant for monocytes, DCs, and neutrophils when analyzed individually (Figure 6B, 6C, 6D). Tumor-associated macrophages (TAMs, defined as CD11b□F4/80□) also showed a trend toward lower CD39 in treated tumors, though variability in the control group prevented significance (Figure 6A). These data align with our in vitro results that IL-27 drives CD39 expression on M-CSF–differentiated macrophages, and extend them to multiple myeloid populations in vivo. By downregulating CD39 on these cells, IL-27 blockade may reduce adenosine accumulation in the tumor, alleviating an important immunosuppressive pathway.

We also observed notable effects on T cells. CD8□ T cells isolated from anti-IL-27-treated tumors had lower surface CD39 levels than those from control tumors (Figure 6E). This was accompanied by a significant decrease in the percentage of CD39□ cells within the CD8□ T cell population (Figure 6F). In the context of tumors, CD8□ T cells that express high levels of CD39 often co-express

other inhibitory receptors (such as PD-1 and TIGIT) and represent an exhausted subset (51,52). Thus, the reduction of CD39 on CD8□ T cells in treated tumors suggests that IL-27 blockade may have curtailed the development of highly exhausted CD8□ T cells, potentially preserving them in a more functional state. Consistent with this, we found that while total CD4□ T cells did not show a change in average CD39 level (Figure 6G), the subset of CD4□ T cells with the highest CD39 expression was significantly reduced in anti-IL-27 tumors (Figure 6H). This subset likely includes regulatory T cells (Tregs), as tumor-infiltrating Tregs characteristically express CD39 and contribute to adenosine-mediated immunosuppression. The frequency of CD39□ cells among CD4□ T cells remained unchanged (Figure 6I), indicating that IL-27 neutralization primarily affected the level of CD39 per cell in CD4□ T cells (especially the most immunosuppressive Tregs), rather than depleting CD39□ T cells altogether.

In summary, IL-27 neutralization in vivo induced changes in the TME consistent with reduced immunosuppression: myeloid cells (monocytes, DCs, neutrophils) showed lower CD39 expression, and T cells (particularly CD8□ effectors) exhibited markers of decreased exhaustion (lower CD39, likely reflecting lower co-expression of other checkpoints like TIGIT). These immune modulations provide a mechanistic basis for the observed tumor growth delay and improved response to checkpoint therapy in IL-27-neutralized tumors.

Discussion

We identify IL-27 as a key regulator of TAM-driven immunosuppression and demonstrate that IL-27 neutralization promotes anti-tumor immunity, at least in part by remodeling myeloid and T-cell compartments within the TME. After demonstrating the presence of IL-27 in monocyte cultures, we showed that macrophages generated in vitro under IL-27 neutralization (Mα27) displayed an intermediate phenotype with reduced levels of protumoral molecules (IL-10, PD-L1, CD155, CD39, CD73, PGE□, CCL22, baseline CCL2) and increased levels of antitumoral ones (GM-CSF, CD40, CD80, CD48). Future studies should evaluate the impact of exogenous IL-27 supplementation on macrophage polarization and delineate the cellular sources and regulatory mechanisms of IL-27 production. Functionally, when in contact with Mα27 macrophages or their secreted factors, CD8□ T cells retained their cytotoxic activity and IFN-γ production, and CD4□ T cells proliferated and secreted more IL-2, unlike their counterparts influenced by control macrophages. These findings suggest that IL-27-neutralized macrophages are less immunosuppressive and more supportive of T cell immunity. In vivo, IL-27 blockade led to reduced tumor growth and extended survival of tumor-bearing mice, especially when combined with PD-L1 blockade. The improved efficacy of combination therapy can be explained by the molecular changes we observed. Notably, IL-27 neutralization inhibited key components of the adenosine pathway in macrophages (CD39 and CD73). These changes likely diminish adenosine accumulation in the TME, which is significant because extracellular adenosine is known to directly suppress T and NK cells and to correlate with poor

responses to ICIs. High expression of CD39, CD73, and A2A adenosine receptors in tumors is associated with worse prognosis and resistance to anti-PD-1/PD-L1 therapy. By downregulating CD39/CD73 and lowering PGE□, IL-27 neutralization may create a more permissive environment for effector T cells, thereby enhancing the impact of PD-L1 blockade. Indeed, therapies targeting the adenosine pathway (CD39/CD73 or adenosine receptors) are currently in clinical trials. Our data indicate that IL-27 is an upstream regulator of this pathway in TAMs, and targeting IL-27 could achieve a similar effect indirectly by "turning off" adenosine production at the source. While our in vivo analyses focused on CD39 (Figure 6), we did not assess CD73 on tumor-infiltrating cells. Given that IL-27 blockade downregulated CD73 on human macrophages in vitro, it is plausible that a similar reduction occurs in vivo, which would further diminish adenosine production in the TME. This will be an important point to verify in future studies.

It is worth noting that IL-27's role in cancer is context-dependent and at times paradoxical (53). A recent study showed that administration of exogenous IL-27 can suppress tumor growth by bolstering CD8□ T cell responses (28). This appears to conflict with our results, which indicate that IL-27 within the tumor favors immunosuppression via macrophages. One possible reconciliation is the difference in IL-27 concentration and timing. Endogenous IL-27 in the TME, likely present at lower levels, may synergize with other factors (e.g., IL-10) to promote a regulatory environment. For instance, IL-27 is known to induce IL-10 production and upregulate PD-L1 and CD39 in various immune cells (27,34,53–55), actions that would support tumor immune escape. In contrast, high-dose IL-27 (from therapeutic administration) can drive potent Th1 and CD8□ T cell activation, overcoming suppressive signals and leading to tumor control (56). This concentration-dependent dualism has been discussed in literature (53). Our findings underscore that, in an established tumor setting rich in immunosuppressive cues, IL-27 predominantly acts as a protumor cytokine by reinforcing TAM-mediated suppression.

Another critical insight from our work is how IL-27 neutralization affects multiple cell types in the TME. While our in vitro study focused on macrophages, the in vivo results indicate a broader impact. We observed decreased CD39 on not only TAMs but also on neutrophils, monocytes, and DCs in the tumors, suggesting IL-27 influences those cells as well. IL-27 receptors are expressed on various immune cells, and IL-27 can directly act on T cells and DCs to modulate their function. For example, IL-27 promotes TIGIT□ regulatory T cell accumulation in some settings (33) and can inhibit DC immunostimulatory capacity (27). Therefore, the improved antitumor immunity we saw with IL-27 blockade likely results from a combination of effects: reprogramming of TAMs and removal of IL-27's direct suppressive influences on T cells and DCs. Our data support a model in which, IL-27 is a central factor sustaining an immunosuppressive network in the TME, and its neutralization causes a network-wide shift toward immunity. Although our working model posits TAM repolarization, we did not quantify canonical polarization markers in tumors (for example NOS2/iNOS, ARG1, and MHC-II), and the decrease in CD39 on TAMs did not reach statistical significance. We therefore

interpret the in vivo data as consistent with a shift toward a less suppressive myeloid milieu rather than definitive evidence of TAM repolarization. Resolving this point will require in situ phenotyping with an expanded polarization panel and orthogonal approaches such as single-cell transcriptomics and spatial multiplex immunohistochemistry.

Our results hold therapeutic implications. They suggest that IL-27 neutralization could be a viable strategy to reprogram the tumor immune microenvironment. Tumors with high macrophage infiltration and elevated IL-27 (or IL-27-inducible genes like ENTPD1/CD39 or IL10) might be especially good candidates for anti-IL-27 therapy. Moreover, combining IL-27 blockade with ICIs (as we tested with anti-PD-L1) appears promising. We noted that IL-27 neutralization led to lower PD-L1 expression on macrophages (as previously shown) and likely on other cells, which might seem counterintuitive when using an anti-PD-L1 drug that targets PD-L1. However, recent studies indicate that reducing PD-L1–mediated suppression (for instance, via downregulation or dual blockade of PD-L1 and another checkpoint) can sometimes enhance overall efficacy of immunotherapy (57). In our case, even if IL-27 blockade slightly reduced PD-L1 levels, the net effect was positive when combined with PD-L1 antibody, probably because the macrophage repolarization and adenosine reduction outweighed any decrease in PD-L1 target density. Additionally, IL-27 blockade diminished TIGIT/CD155 signaling (by reducing CD155 on myeloid cells and $CD39^{high}$ Treg frequency), which is another pathway of immunotherapy resistance (58). Indeed, high CD155 in tumors has been linked to poor outcomes and lack of response to ICIs (59), and blocking TIGIT is being actively explored clinically (58). By lowering CD155 on TAMs and other myeloid cells, IL-27 neutralization might synergize with TIGIT or PD-1/PD-L1 targeting.

In conclusion, we identify IL-27 as a key regulator of TAM-driven immunosuppression and demonstrate that IL-27 neutralization can repolarize macrophages to a state that supports anti-tumor immunity. IL-27 blockade slows tumor growth and enhances the efficacy of immune checkpoint blockade in our model, providing a strong rationale for clinical investigation of IL-27–targeted therapies. Our findings contribute to the understanding of how modulating a single cytokine (IL-27) can orchestrate multiple immunosuppressive mechanisms in the TME, and they highlight the potential of IL-27 neutralization as a novel immunotherapeutic approach in cancer.

Figure Legends

Figure 1. IL-27 neutralization during macrophage differentiation remodels phenotype. Macrophages were differentiated for 7 days with M-CSF alone (Untreated), M-CSF + αIL-27 antibody (αIL-27 Ab), or M-CSF + isotype-matched control IgG (Control Ab). (A) CD73 protein (representative donor) quantified by western blot. (B) Paired comparison of CD73 protein levels relative to Untreated (Wilcoxon matched-pairs signed-rank test). (C–F) Surface expression of immunomodulatory molecules (CD155, CD80, CD40, CD48) by flow cytometry on CD14□ gated cells. (G–H) Secreted CCL2 and CCL22 after 24 h culture (ELISA). (I–J) After 24 h LPS stimulation,

secreted PGE□ and GM-CSF (ELISA). (K) Heatmap summarizing significant phenotype changes with IL-27 neutralization. Flow-cytometry data are shown as relative fluorescence intensity (RFI) = MFI_specific / MFI_isotype; qRT-PCR as mRNA normalized to GAPDH; ELISA in ng/mL. Each dot = an independent experiment. Data are mean ± SEM. Statistics: one-way ANOVA with Tukey's post-hoc; paired Wilcoxon for panel B. Significance: $p < 0.05$ (*$p < 0.05$; **$p < 0.01$; ***$p < 0.001$).

Figure 2. IL-27 neutralization alters macrophage metabolism. (A–C) Oxygen consumption rate (OCR) parameters from Seahorse XF Cell Mito Stress Test, namely basal respiration, maximal respiration, ATP-linked respiration, in macrophages differentiated with M-CSF or GM-CSF. (D–E) Extracellular acidification rate (ECAR) parameters from Glycolysis Stress Test, namely glycolysis and glycolytic capacity, in M-CSF vs GM-CSF conditions. (F) Lactate concentration (supernatants) in M-CSF vs GM-CSF macrophages. (G, I) OCR parameters (basal, ATP-linked) in Miso vs Mα27 macrophages. (H) Basal ECAR in Miso vs Mα27. (J) Lactate concentration in Miso vs Mα27. Each dot = an independent experiment; mean ± SEM. Statistics: unpaired two-tailed Student's ***t***-test (GraphPad Prism 10) for all two-group comparisons. Significance: $\boldsymbol{p} < 0.05$ (*).

Figure 3. IL-27 neutralization restores macrophage support for T-cell activation and cytotoxicity. Macrophages (Untreated, αIL-27 Ab, Control Ab) were extensively washed and then LPS-activated for 24 h to generate M-CM; matched isotype IgG was included in all cultures. (A) IFN-γ secretion by activated CD8□ T cells cultured with 10% macrophage M-CM (ELISA). (B) Macrophage effects on the cytotoxicity of a MUC1-specific CD8□ T-cell clone after 72 h co-culture with tumor targets. Macrophages were differentiated with M-CSF (Untreated), M-CSF + αIL-27 Ab, or M-CSF + isotype control (Control Ab), washed, and then added to T cells and targets. Cytotoxicity is shown as the percent change in tumor-cell lysis relative to the no-macrophage control (set to 0%); negative values indicate suppression and positive values enhancement. (C) IL-2 secretion by activated CD4□ T cells cultured with 10% M-CM (ELISA). (D) Impact of 10% M-CM on CD4□ T-cell replication index after 6 days (CFDA-SE dilution by flow cytometry). ELISA in ng/mL. Each dot = an independent experiment; mean ± SEM. Statistics: one-way ANOVA with Tukey's post-hoc. Significance: $p < 0.05$ (*).

Figure 4. Therapeutic efficacy of anti-IL-27 in MC38 tumors. (A) 5×10^5 MC38 cells injected s.c. in the right flank of C57BL/6 mice. Eight days later (D0), mice received intratumoral αIL-27 or isotype-matched control IgG every 48 h (D0, D2, D4, D6, D8; five doses total). Tumor monitoring ended when the first tumor reached 1,800 mm^3 (D10); survival follow-up ended at D22 when the last tumor reached 1,800 mm^3. (B–C) Individual tumor-growth spaghetti plots by treatment arm (αIL-27 vs Control Ab). (D) Cumulative mean tumor volumes (± SEM) every two days. (E) Tumor volumes measured on D0 (treatment start), D4, and D10. (F) Kaplan–Meier survival of MC38-bearing mice by treatment. Each symbol = one mouse. Data pooled from two independent experiments; mean ± SEM. Statistics: one-way ANOVA with Tukey's post-hoc for volumes; log-rank (Mantel–Cox) for survival (overall $p = 0.008$). Significance: $p < 0.05$ (*$p<0.05$, **$p<0.01$).

Figure 5. Combination therapy: anti-IL-27 enhances response to anti-PD-L1. (A) MC38 model as in Figure 4. After five intratumoral doses of αIL-27 or isotype control (D0–D8), anti-PD-L1 was started 2 days later (i.p. every 3 days on D9, D12, D15). Tumor monitoring ended when the first tumor reached 1,800 mm³ (D15); survival follow-up ended at D31. (B) Tumor volumes at D15 by treatment group. (C) Kaplan–Meier survival by treatment group. Each symbol = one mouse. Data pooled from two independent experiments; mean ± SEM. Statistics: one-way ANOVA with Tukey's post-hoc for volumes; log-rank for survival (exact p values annotated on the plot; e.g., *p = 0.04; **p = 0.002). Significance: $p < 0.05$ (*).

Figure 6. IL-27 neutralization lowers CD39 on tumor-infiltrating immune cells. Upon tumors reaching 20–50 mm³ (~day 8), mice received intratumoral αIL-27 or isotype control every 48 h (D0, D2, D4, D6, D8). Tumors were harvested on day 10 for flow cytometry. (A) Box plots of gMFI (geometric MFI) for CD39 across myeloid subsets. (B–D) CD39 gMFI on neutrophils, dendritic cells, and monocytes. (E) CD39 gMFI on infiltrating CD8□ T cells. (F) Frequency of CD39□ cells among CD8□ T cells. (G) CD39 gMFI on infiltrating CD4□ T cells. (H) CD39 gMFI on CD4□ T cells within the CD39^{high} subset. (I) Frequency of CD39□ cells among CD4□ T cells. Each symbol = one mouse. Data pooled from two independent experiments; mean ± SEM. Statistics: Mann–Whitney tests. Significance: $p < 0.05$ (*p<0.05, **p<0.01).

Supplementary Figure legends :

Supplementary Figure 1. Expression and secretion of IL-27 by human monocytes and macrophages. mRNA expression of IL-27 subunits (IL-27p28, Ebi3) and receptor subunits (IL-27RA, gp130) in monocytes prior to differentiation, quantified by RT-qPCR and normalized to GAPDH (A). Induction of IL-27p28 and IL-27RA transcripts in monocytes after 5 days of differentiation with M-CSF, assessed by RT-qPCR and normalized to GAPDH (B). IL-27p28 concentration in culture supernatants of monocytes and macrophages, with or without LPS stimulation, measured by ELISA (C). Membrane-associated IL-27p28 in unstimulated monocytes, measured by ELISA (D). Membrane-associated IL-27p28 during macrophage differentiation (day 0 to day 5, M-CSF), measured by ELISA (E).Results are expressed as mean ± SEM of independent experiments.

Supplementary Figure 2. CD39 expression on macrophages after treatment with immunomodulatory compounds. Macrophages differentiated for 7 days with M-CSF were exposed to the following modulators: (A) the adenosine receptor antagonist caffeine, (B) the EP2 receptor antagonist AH6809, and (C) GM-CSF. Surface CD39 was quantified by flow cytometry. Results are expressed as relative fluorescence intensity (RFI), calculated as MFI_specific / MFI_isotype (isotype-matched control). Each dot represents an independent experiment; data are mean ± SEM. Statistics: one-way ANOVA with Tukey's post-hoc test (two-tailed; $\alpha = 0.05$). Significance: $p < 0.05$ *(*p<0.05, **p<0,01, ****p<0,0001).*

Supplementary Figure 3. IL-27 neutralization during macrophage differentiation modifies phenotype. Macrophages were generated for 7 days with M-CSF (Untreated), M-CSF + **α**IL-27 antibody (**α**IL-27 Ab), or M-CSF + isotype-matched IgG (Control Ab). (A) *NT5E* (CD73) mRNA by RT-qPCR (normalized to GAPDH). (B) CCL2 secreted after 24 h LPS stimulation (ELISA), (C) CCL2 secreted by inflammatory macrophages (with and without activation step), (D) IL-10 secreted after 24 h LPS stimulation (ELISA). (E) *PTGS2* (COX-2) mRNA by RT-qPCR. (F) COX-2 protein by western blot (representative donor). (G) Paired comparison of COX-2 protein levels relative to Untreated. Each dot represents an independent experiment; data are mean ± SEM. Statistics: one-way ANOVA with Tukey's post-hoc test (paired analysis used where donor-matched). Significance: $p < 0.05$ (*p<0.05, **p<0,01).

Supplementary Figure 4. Macrophage conditioned medium inhibits IFN-γ secretion by CD8 T cells. In the indicated condition, LPS-activated M-CM of untreated macrophages (10% of total volume) was added to cultures of $CD8^+$ T cells along with PHA at 10 µg/mL for 48 h. In Mock condition no conditioned medium was added. IFN-γ in culture supernatants (ELISA). Each dot represents an independent experiment; data are mean ± SEM. Statistics: one-way ANOVA with Tukey's post-hoc test (two-tailed; α = 0.05). Significance: $p < 0.05$ (*).

Supplementary Figure 5. Gating strategy for flow-cytometry analysis of the tumor microenvironment. C57BL/6 mice bearing subcutaneous MC38 tumors were analyzed by flow cytometry 10 days after inoculation. The figure shows the gating sequence used to identify tumor-infiltrating macrophages, monocytes, neutrophils, dendritic cells, CD4 T cells, and CD8 T cells. A representative experiment is shown. Analysis was performed in FlowJo v10; instrument details are provided in Methods.

Acknowledgements

We thank all members of mice core facilities (UMS006, ANEXPLO, Inserm, Toulouse) for their support and technical assistance. We thank Dominique Rozet for the daily help on the administrative and financial management of our team. The authors are grateful to the CRCI2NA technical platforms for the support and to the We-Met platform for the Seahorse analysis. Flow cytometry experiments were done at the INFINITy-INSERM UMR1291 core facility connected to the Toulouse Réseau Imagerie network, member of the France-BioImaging national infrastructure supported by the French National Research Agency (ANR-10-INBS-04). We thank all team members for their availability and help.

References

1. Lei Q, Wang D, Sun K, Wang L, Zhang Y. Resistance Mechanisms of Anti-PD1/PDL1 Therapy in Solid Tumors. Front Cell Dev Biol. 21 juill 2020;8:672.

2. Kluger HM, Tawbi HA, Ascierto ML, Bowden M, Callahan MK, Cha E, et al. Defining tumor resistance to PD-1 pathway blockade: recommendations from the first meeting of the SITC Immunotherapy Resistance Taskforce. J Immunother Cancer. 1 mars 2020;8(1):e000398.

3. Nengroo MA, Verma A, Datta D. Cytokine chemokine network in tumor microenvironment: Impact on CSC properties and therapeutic applications. Cytokine. 1 août 2022;156:155916.

4. Babar Q, Saeed A, Tabish TA, Sarwar M, Thorat ND. Targeting the tumor microenvironment: Potential strategy for cancer therapeutics. Biochimica et Biophysica Acta (BBA) - Molecular Basis of Disease. 1 août 2023;1869(6):166746.

5. Mantovani A, Allavena P, Marchesi F, Garlanda C. Macrophages as tools and targets in cancer therapy. Nat Rev Drug Discov. nov 2022;21(11):799□820.

6. Bied M, Ho WW, Ginhoux F, Blériot C. Roles of macrophages in tumor development: a spatiotemporal perspective. Cell Mol Immunol. sept 2023;20(9):983□92.

7. Kerneur C, Cano CE, Olive D. Major pathways involved in macrophage polarization in cancer. Frontiers in Immunology [Internet]. 2022 [cité 21 nov 2023];13. Disponible sur: https://www.frontiersin.org/articles/10.3389/fimmu.2022.1026954

8. Christofides A, Strauss L, Yeo A, Cao C, Charest A, Boussiotis VA. The complex role of tumor-infiltrating macrophages. Nat Immunol. août 2022;23(8):1148□56.

9. Li M, He L, Zhu J, Zhang P, Liang S. Targeting tumor-associated macrophages for cancer treatment. Cell & Bioscience. 7 juin 2022;12(1):85.

10. Argyle D, Kitamura T. Targeting Macrophage-Recruiting Chemokines as a Novel Therapeutic Strategy to Prevent the Progression of Solid Tumors. Frontiers in immunology [Internet]. 13 nov 2018 [cité 21 nov 2023];9. Disponible sur: http://pubmed.ncbi.nlm.nih.gov/30483271/

11. Bejarano L, Jordão MJC, Joyce JA. Therapeutic Targeting of the Tumor Microenvironment. Cancer Discovery. 1 avr 2021;11(4):933□59.

12. Ries CH, Cannarile MA, Hoves S, Benz J, Wartha K, Runza V, et al. Targeting tumor-associated macrophages with anti-CSF-1R antibody reveals a strategy for cancer therapy. Cancer Cell. 16 juin 2014;25(6):846□59.

13. Kowal J, Kornete M, Joyce JA. Re-education of macrophages as a therapeutic strategy in cancer. Immunotherapy. juin 2019;11(8):677□89.

14. van Dalen FJ, van Stevendaal MHME, Fennemann FL, Verdoes M, Ilina O. Molecular Repolarisation of Tumour-Associated Macrophages. Molecules [Internet]. 20 déc 2018 [cité 26 mars 2020];24(1). Disponible sur: https://www.ncbi.nlm.nih.gov/pmc/articles/PMC6337345/

15. Van der Jeught K, Bialkowski L, Daszkiewicz L, Broos K, Goyvaerts C, Renmans D, et al. Targeting the tumor microenvironment to enhance antitumor immune responses. Oncotarget. 26 déc 2014;6(3):1359□81.

16. d'Almeida SM, Kauffenstein G, Roy C, Basset L, Papargyris L, Henrion D, et al. The ecto-ATPDase CD39 is involved in the acquisition of the immunoregulatory phenotype by M-CSF-

macrophages and ovarian cancer tumor-associated macrophages: Regulatory role of IL-27. Oncoimmunology. juill 2016;5(7):e1178025.

17. Montalbán Del Barrio I, Penski C, Schlahsa L, Stein RG, Diessner J, Wöckel A, et al. Adenosine-generating ovarian cancer cells attract myeloid cells which differentiate into adenosine-generating tumor associated macrophages - a self-amplifying, CD39- and CD73-dependent mechanism for tumor immune escape. J Immunother Cancer. 2016;4:49.

18. Chiarella AM, Ryu YK, Manji GA, Rustgi AK. Extracellular ATP and Adenosine in Cancer Pathogenesis and Treatment. Trends in Cancer. 1 août 2021;7(8):731□50.

19. Kashyap AS, Thelemann T, Klar R, Kallert SM, Festag J, Buchi M, et al. Antisense oligonucleotide targeting CD39 improves anti-tumor T cell immunity. J Immunother Cancer. 12 2019;7(1):67.

20. Park YJ, Ryu H, Choi G, Kim BS, Hwang ES, Kim HS, et al. IL-27 confers a protumorigenic activity of regulatory T cells via CD39. Proc Natl Acad Sci U S A. 19 févr 2019;116(8):3106□11.

21. Perrot I, Michaud HA, Giraudon-Paoli M, Augier S, Docquier A, Gros L, et al. Blocking Antibodies Targeting the CD39/CD73 Immunosuppressive Pathway Unleash Immune Responses in Combination Cancer Therapies. Cell Reports. 21 mai 2019;27(8):2411-2425.e9.

22. Liu Y, Li Z, Zhao X, Xiao J, Bi J, Li XY, et al. Review immune response of targeting CD39 in cancer. Biomark Res. déc 2023;11(1):1□12.

23. Guo S, Han F, Zhu W. CD39 – A bright target for cancer immunotherapy. Biomedicine & Pharmacotherapy. 1 juill 2022;151:113066.

24. Vigano S, Alatzoglou D, Irving M, Ménétrier-Caux C, Caux C, Romero P, et al. Targeting Adenosine in Cancer Immunotherapy to Enhance T-Cell Function. Front Immunol. 6 juin 2019 ;10. Disponible sur: https://www.ncbi.nlm.nih.gov/pmc/articles/PMC6562565/

25. Vijayan D, Young A, Teng MWL, Smyth MJ. Targeting immunosuppressive adenosine in cancer. Nat Rev Cancer. 22 2017;17(12):765.

26. Alameddine J, Godefroy E, Papargyris L, Sarrabayrouse G, Tabiasco J, Bridonneau C, et al. Faecalibacterium prausnitzii Skews Human DC to Prime IL10-Producing T Cells Through TLR2/6/JNK Signaling and IL-10, IL-27, CD39, and IDO-1 Induction. Front Immunol. 2019;10:143.

27. Mascanfroni ID, Yeste A, Vieira SM, Burns EJ, Patel B, Sloma I, et al. Interleukin-27 acts on dendritic cells to suppress the T-cell response and autoimmunity by inducing the expression of ENTPD1 (CD39). Nat Immunol. oct 2013;14(10):1054□63.

28. Bréart B, Williams K, Krimm S, Wong T, Kayser B, Wang L, et al. IL-27 elicits a cytotoxic CD8 T cell program to enforce tumour control. Nature. 5 févr 2025;639:746□53.

29. Xu H, Wang G, Zhu L, Liu H, Li B. Eight immune-related genes predict survival outcomes and immune characteristics in breast cancer. Aging (Albany NY). 3 août 2020;12(16):16491□513.

30. Li P, Pu S, Yi J, Li X, Wu Q, Yang C, et al. Deletion of IL-27p28 induces CD8 T cell immunity against colorectal tumorigenesis. International Immunopharmacology. 15 févr 2024;128:111464.

31. Dusi S, Bronte V, De Sanctis F. IL-27: overclocking cytotoxic T lymphocytes to boost cancer immunotherapy. Sig Transduct Target Ther. 21 avr 2025;10(1):126.

32. Maleki AH, Rajabivahid M, Khosh E, Khanali Z, Tahmasebi S, Ghorbi MD. Harnessing IL-27: challenges and potential in cancer immunotherapy. Clin Exp Med. 2025;25(1):34.

33. Chihara N, Madi A, Kondo T, Zhang H, Acharya N, Singer M, et al. Induction and transcriptional regulation of the co-inhibitory gene module in T cells. Nature. juin 2018;558(7710):454–9.

34. Carbotti G, Barisione G, Airoldi I, Mezzanzanica D, Bagnoli M, Ferrero S, et al. IL-27 induces the expression of IDO and PD-L1 in human cancer cells. Oncotarget. 22 déc 2015;6(41):43267–80.

35. Chen YC, Lai YS, Hsuuw YD, Chang KT. Withholding of M-CSF Supplement Reprograms Macrophages to M2-Like via Endogenous CSF-1 Activation. Int J Mol Sci. 29 mars 2021;22(7):3532.

36. Becker M, De Bastiani MA, Parisi MM, Guma FTCR, Markoski MM, Castro MAA, et al. Integrated Transcriptomics Establish Macrophage Polarization Signatures and have Potential Applications for Clinical Health and Disease. Sci Rep. 25 août 2015;5(1):13351.

37. Achard C, Guillerme JB, Bruni D, Boisgerault N, Combredet C, Tangy F, et al. Oncolytic measles virus induces tumor necrosis factor-related apoptosis-inducing ligand (TRAIL)-mediated cytotoxicity by human myeloid and plasmacytoid dendritic cells. Oncoimmunology. 18 nov 2016;6(1):e1261240.

38. Zhou R, Chen S, Wu Q, Liu L, Wang Y, Mo Y, et al. CD155 and its receptors in cancer immune escape and immunotherapy. Cancer Letters. 1 oct 2023;573:216381.

39. Solomon BL, Garrido-Laguna I. TIGIT: a novel immunotherapy target moving from bench to bedside. Cancer Immunol Immunother. 1 nov 2018;67(11):1659–67.

40. Kučan Brlić P, Lenac Roviš T, Cinamon G, Tsukerman P, Mandelboim O, Jonjić S. Targeting PVR (CD155) and its receptors in anti-tumor therapy. Cell Mol Immunol. janv 2019;16(1):40–52.

41. Marin-Acevedo JA, Dholaria B, Soyano AE, Knutson KL, Chumsri S, Lou Y. Next generation of immune checkpoint therapy in cancer: new developments and challenges. J Hematol Oncol [Internet]. 15 mars 2018 [cité 31 mars 2020];11. Disponible sur: https://www.ncbi.nlm.nih.gov/pmc/articles/PMC5856308/

42. Ara A, Ahmed KA, Xiang J. Multiple effects of CD40–CD40L axis in immunity against infection and cancer. Immunotargets Ther. 28 juin 2018;7:55–61.

43. Xia S, Wei J, Wang J, Sun H, Zheng W, Li Y, et al. A requirement of dendritic cell-derived interleukin-27 for the tumor infiltration of regulatory T cells. Journal of Leukocyte Biology. 2014;95(5):733–42.

44. Take Y, Koizumi S, Nagahisa A. Prostaglandin E Receptor 4 Antagonist in Cancer Immunotherapy: Mechanisms of Action. Front Immunol [Internet]. 10 mars 2020 [cité 31 mars 2020];11. Disponible sur: https://www.ncbi.nlm.nih.gov/pmc/articles/PMC7076081/

45. Foucher ED, Blanchard S, Preisser L, Descamps P, Ifrah N, Delneste Y, et al. IL-34- and M-CSF-induced macrophages switch memory T cells into Th17 cells via membrane IL-1α. Eur J Immunol. avr 2015;45(4):1092□102.

46. Vijayan V, Pradhan P, Braud L, Fuchs HR, Gueler F, Motterlini R, et al. Human and murine macrophages exhibit differential metabolic responses to lipopolysaccharide - A divergent role for glycolysis. Redox Biology. 1 avr 2019;22:101147.

47. Wculek SK, Dunphy G, Heras-Murillo I, Mastrangelo A, Sancho D. Metabolism of tissue macrophages in homeostasis and pathology. Cell Mol Immunol. mars 2022;19(3):384□408.

48. Kruglov V, Jang IH, Camell CD. Inflammaging and fatty acid oxidation in monocytes and macrophages. Immunometabolism (Cobham). janv 2024;6(1):e00038.

49. Koo SJ, Garg N. Metabolic programming of macrophage functions and pathogens control. Redox Biology. 1 avr 2019;24:101198.

50. Roulois D, Vignard V, Gueugnon F, Labarrière N, Grégoire M, Fonteneau JF. Recognition of pleural mesothelioma by mucin-1(950–958)/human leukocyte antigen A*0201-specific CD8+ T-cells. European Respiratory Journal. 1 nov 2011;38(5):1117□26.

51. Gerhardt L, Hong MMY, Yousefi Y, Figueredo R, Maleki Vareki S. IL-12 and IL-27 Promote CD39 Expression on CD8+ T Cells and Differentially Regulate the CD39+CD8+ T Cell Phenotype. J Immunol. 15 mai 2023;210(10):1598□606.

52. Canale FP, Ramello MC, Núñez N, Furlan CLA, Bossio SN, Serrán MG, et al. CD39 Expression Defines Cell Exhaustion in Tumor-Infiltrating CD8+ T Cells. Cancer Research. 2 janv 2018;78(1):115□28.

53. Fabbi M, Carbotti G, Ferrini S. Dual Roles of IL-27 in Cancer Biology and Immunotherapy. Mediators of Inflammation.

54. Awasthi A, Carrier Y, Peron JPS, Bettelli E, Kamanaka M, Flavell RA, et al. A dominant function for interleukin 27 in generating interleukin 10–producing anti-inflammatory T cells. Nat Immunol. déc 2007;8(12):1380□9.

55. Zhu C, Sakuishi K, Xiao S, Sun Z, Zaghouani S, Gu G, et al. An IL-27/NFIL3 signaling axis drives Tim-3 and IL-10 expression and T cell dysfunction. Nat Commun. 23 janv 2015;6:6072.

56. Ding M, Fei Y, Zhu J, Ma J, Zhu G, Zhen N, et al. IL□27 improves adoptive CD8+ T cells' antitumor activity via enhancing cell survival and memory T cell differentiation. Cancer Sci. juill 2022;113(7):2258□71.

57. Yi M, Niu M, Xu L, Luo S, Wu K. Regulation of PD-L1 expression in the tumor microenvironment. Journal of Hematology & Oncology. 7 janv 2021;14(1):10.

58. Kawashima S, Inozume T, Kawazu M, Ueno T, Nagasaki J, Tanji E, et al. TIGIT/CD155 axis mediates resistance to immunotherapy in patients with melanoma with the inflamed tumor microenvironment. J Immunother Cancer. 1 mai 2022;9(11):e003134.

59. Jiang C, Qu X, Ma L, Yi L, Cheng X, Gao X, et al. CD155 expression impairs anti-PD1 therapy response in non-small cell lung cancer. Clin Exp Immunol. 11 juin 2022;208(2):220–32.

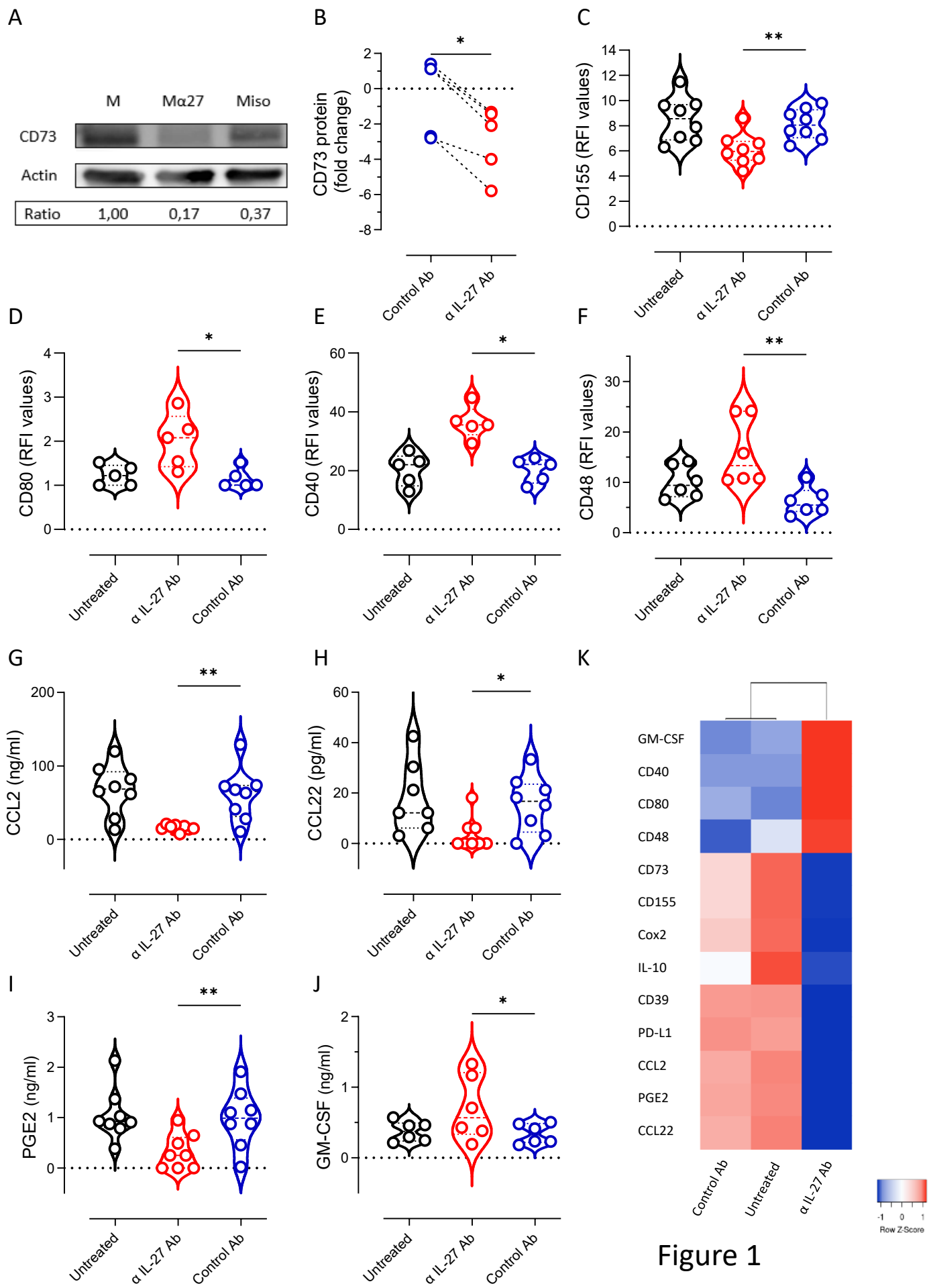
A
M
Mα27
Miso
CD73
Actin
Ratio
1,00
0,17
0,37
B
CD73 protein (fold change)
Control Ab
α IL-27 Ab
C
CD155 (RFI values)
Untreated
α IL-27 Ab
Control Ab
D
CD80 (RFI values)
E
CD40 (RFI values)
F
CD48 (RFI values)
G
CCL2 (ng/ml)
H
CCL22 (pg/ml)
I
PGE2 (ng/ml)
J
GM-CSF (ng/ml)
K
GM-CSF
CD40
CD80
CD48
CD73
CD155
Cox2
IL-10
CD39
PD-L1
CCL2
PGE2
CCL22
Row Z-Score

Figure 1

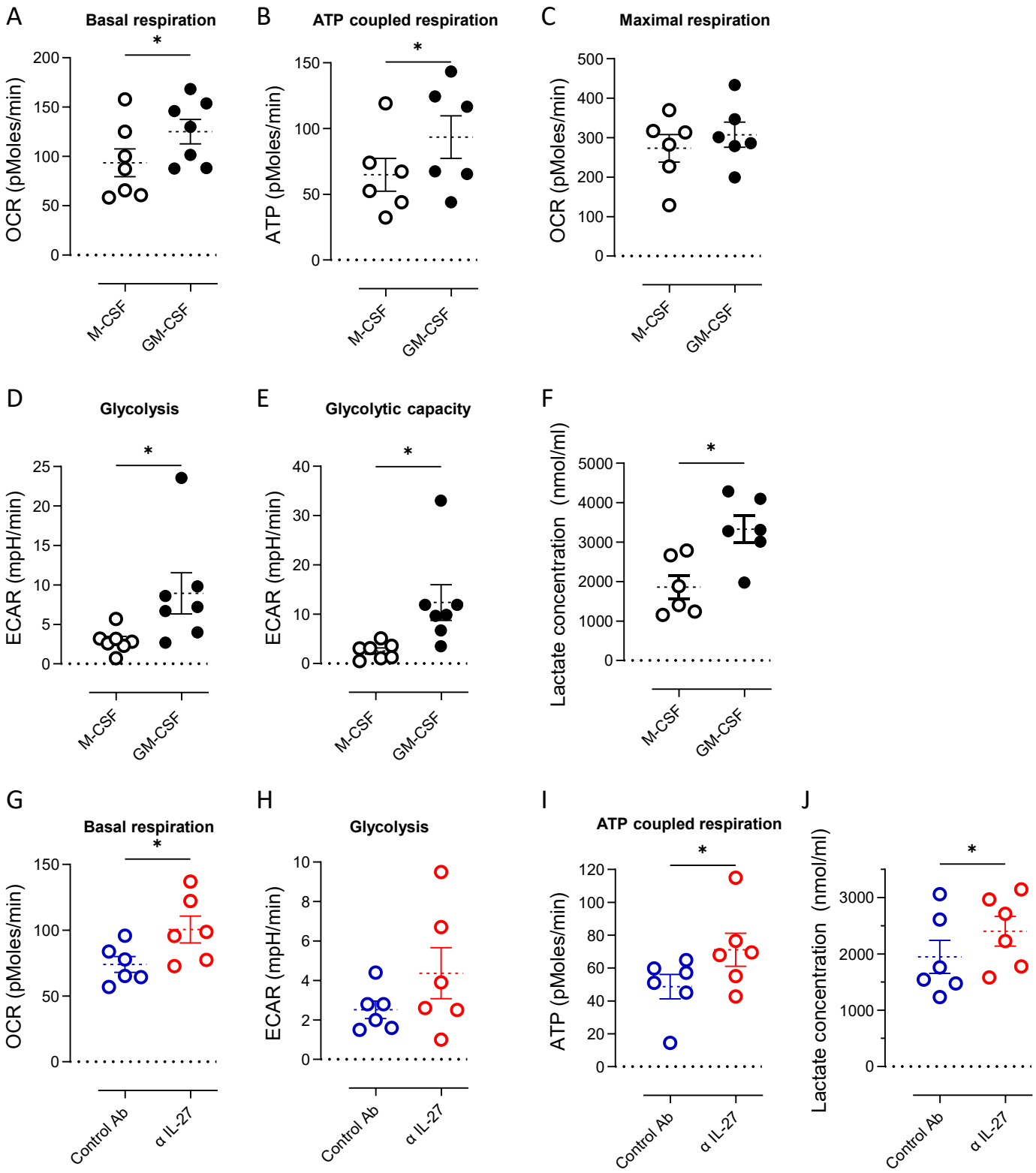
A
Basal respiration
OCR (pMoles/min)
200
150
100
50
0
*
M-CSF
GM-CSF
B
ATP coupled respiration
ATP (pMoles/min)
150
100
50
0
*
M-CSF
GM-CSF
C
Maximal respiration
OCR (pMoles/min)
500
400
300
200
100
0
M-CSF
GM-CSF
D
Glycolysis
ECAR (mpH/min)
25
20
15
10
5
0
*
M-CSF
GM-CSF
E
Glycolytic capacity
ECAR (mpH/min)
40
30
20
10
0
*
M-CSF
GM-CSF
F
Lactate concentration (nmol/ml)
5000
4000
3000
2000
1000
0
*
M-CSF
GM-CSF
G
Basal respiration
OCR (pMoles/min)
150
100
50
0
*
Control Ab
α IL-27
H
Glycolysis
ECAR (mpH/min)
10
8
6
4
2
0
Control Ab
α IL-27
I
ATP coupled respiration
ATP (pMoles/min)
120
100
80
60
40
20
0
*
Control Ab
α IL-27
J
Lactate concentration (nmol/ml)
3000
2000
1000
0
*
Control Ab
α IL-27

Figure 2

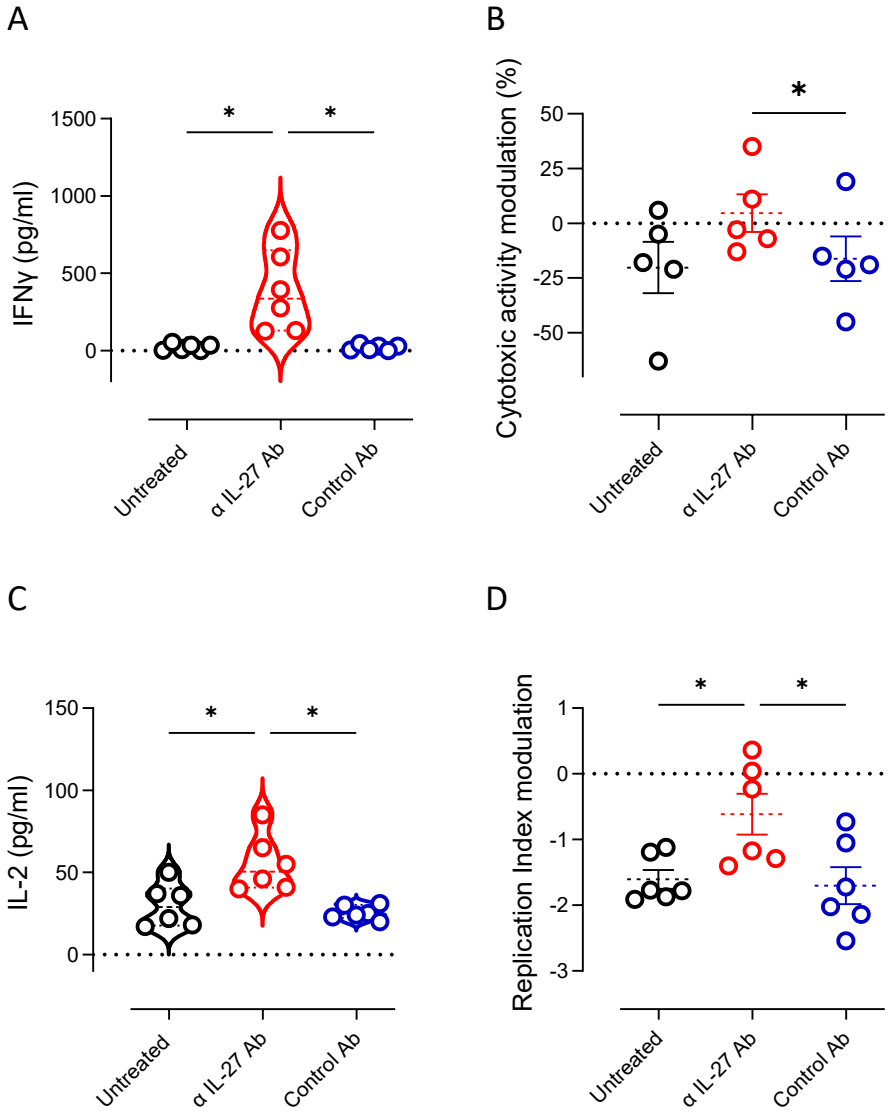
A
IFNγ (pg/ml)
1500
1000
500
0
*
*
Untreated
α IL-27 Ab
Control Ab
B
Cytotoxic activity modulation (%)
50
25
0
-25
-50
*
Untreated
α IL-27 Ab
Control Ab
C
IL-2 (pg/ml)
150
100
50
0
*
*
Untreated
α IL-27 Ab
Control Ab
D
Replication Index modulation
1
0
-1
-2
-3
*
*
Untreated
α IL-27 Ab
Control Ab

Figure 3

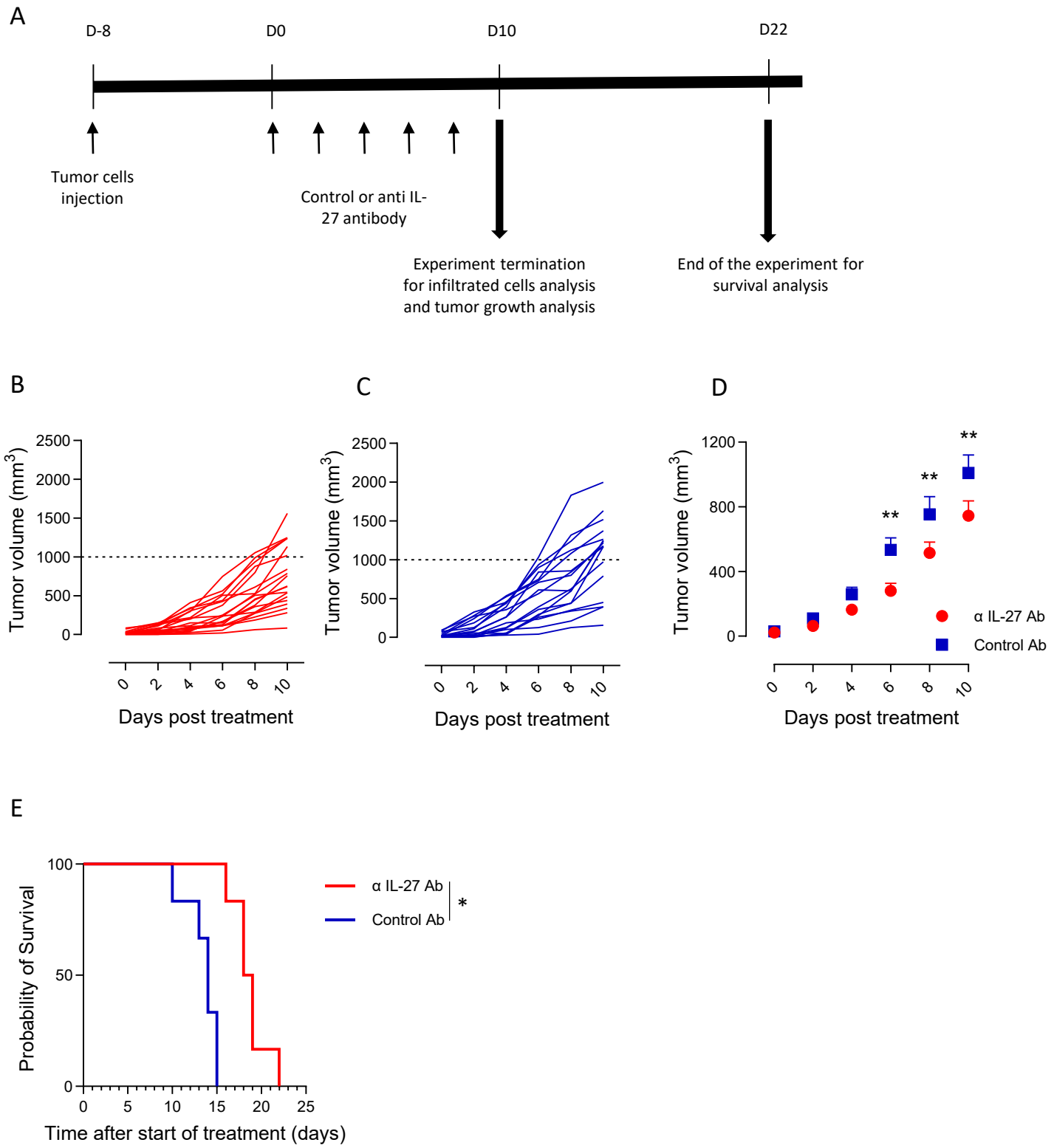
A
D-8
D0
D10
D22
Tumor cells injection
Control or anti IL-27 antibody
Experiment termination for infiltrated cells analysis and tumor growth analysis
End of the experiment for survival analysis
B
C
D
Tumor volume (mm3)
Days post treatment
α IL-27 Ab
Control Ab
**
E
Probability of Survival
Time after start of treatment (days)
*

Figure 4

A

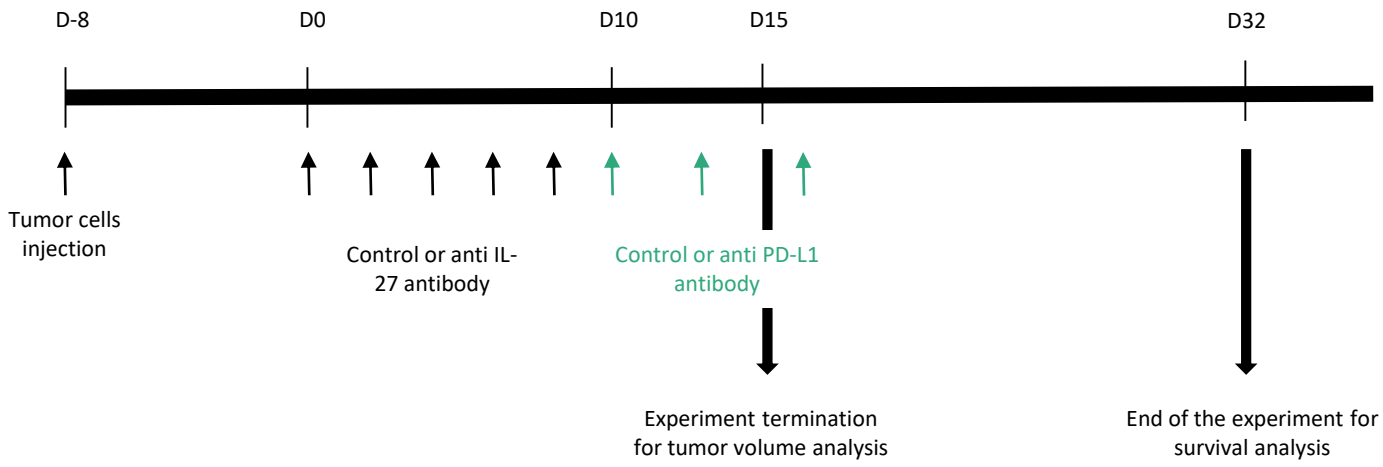
D-8
D0
D10
D15
D32
Tumor cells injection
Control or anti IL-27 antibody
Control or anti PD-L1 antibody
Experiment termination for tumor volume analysis
End of the experiment for survival analysis

B

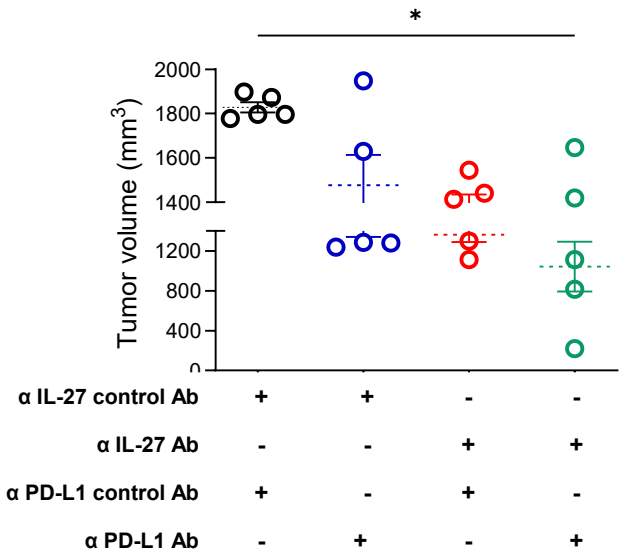
*
Tumor volume (mm3)
2000
1800
1600
1400
1200
800
400
0
α IL-27 control Ab + + - -
α IL-27 Ab - - + +
α PD-L1 control Ab + - + -
α PD-L1 Ab - + - +

C

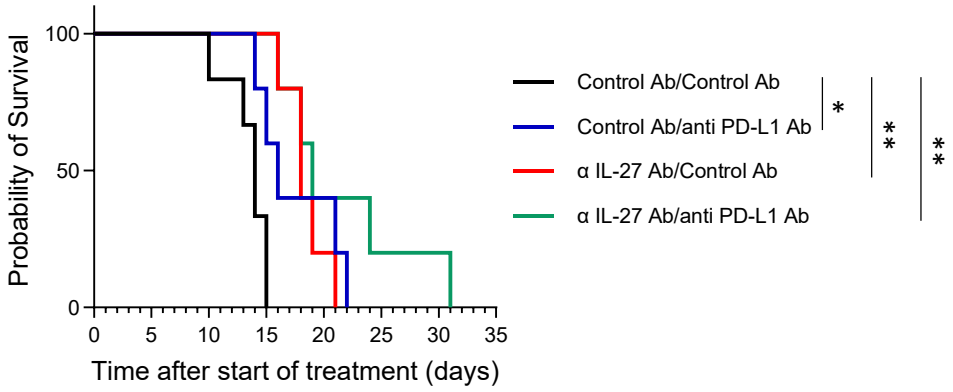
Probability of Survival
100
50
0
0 5 10 15 20 25 30 35
Time after start of treatment (days)
Control Ab/Control Ab
Control Ab/anti PD-L1 Ab
α IL-27 Ab/Control Ab
α IL-27 Ab/anti PD-L1 Ab
*
**
**

Figure 5

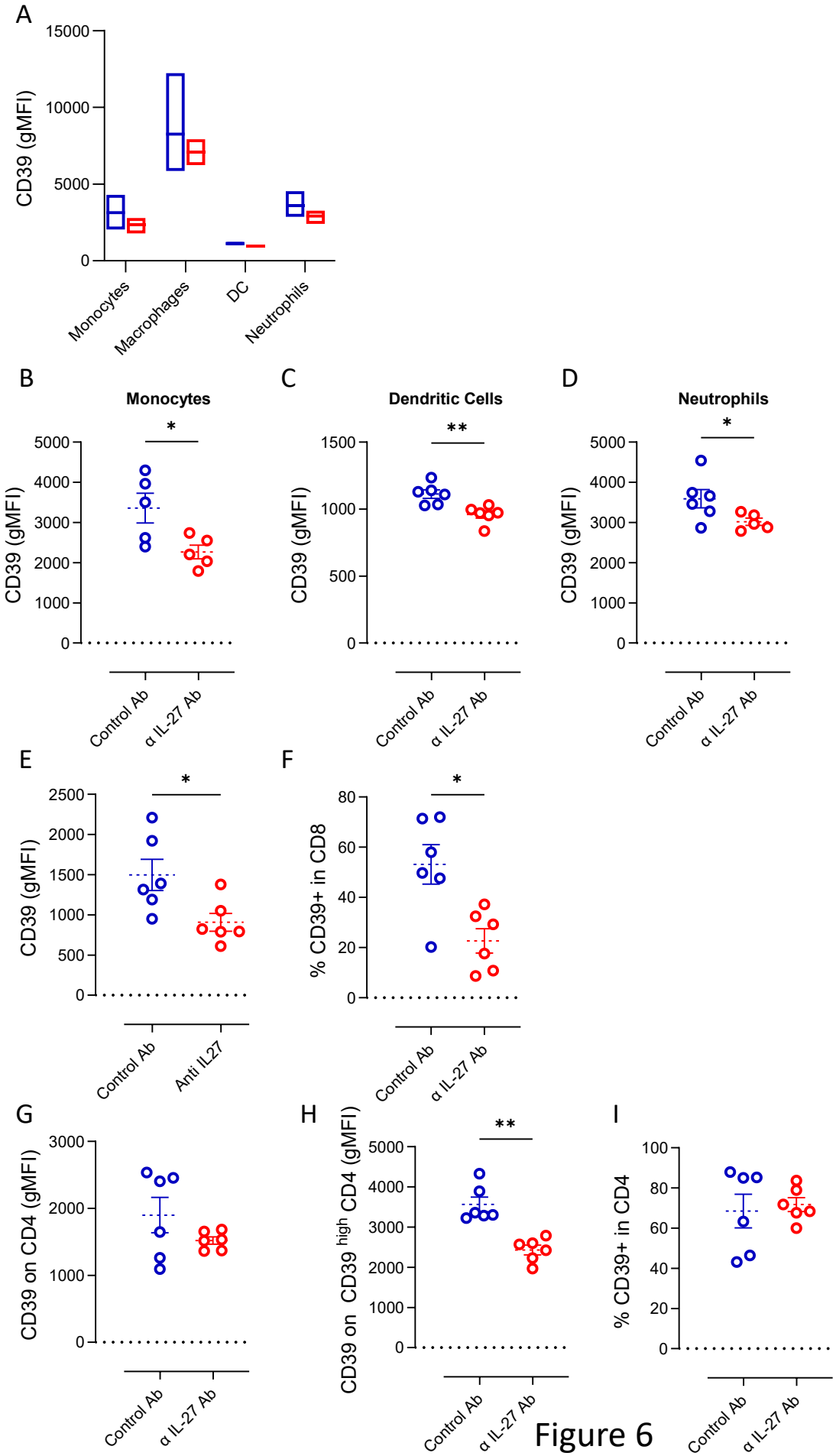
A
CD39 (gMFI)
15000
10000
5000
0
Monocytes
Macrophages
DC
Neutrophils
B
Monocytes
CD39 (gMFI)
*
Control Ab
α IL-27 Ab
C
Dendritic Cells
CD39 (gMFI)
**
Control Ab
α IL-27 Ab
D
Neutrophils
CD39 (gMFI)
*
Control Ab
α IL-27 Ab
E
CD39 (gMFI)
*
Control Ab
Anti IL27
F
% CD39+ in CD8
*
Control Ab
α IL-27 Ab
G
CD39 on CD4 (gMFI)
Control Ab
α IL-27 Ab
H
CD39 on CD39 high CD4 (gMFI)
**
Control Ab
α IL-27 Ab
I
% CD39+ in CD4
Control Ab
α IL-27 Ab

Figure 6